Advanced Composite Materials
Publication details, including instructions for authors and subscription information:
http://www.tandfonline.com/loi/tacm20

Visco-plastic analysis of adhesively bonded joints in composite materials

S.C. Pradhan [a] , N.N. Kishore [b] & N.G.R. Iyengar [c]
[a] Structural Sciences Division, National Aerospace Laboratories, Bangalore 560 017, India
[b] Mechanical Engineering Department, Indian Institute of Technology, Kanpur 208 016, India
[c] Aerospace Engineering Department, Indian Institute of Technology, Kanpur 208 016, India
Version of record first published: 02 Apr 2012.

To cite this article: S.C. Pradhan , N.N. Kishore & N.G.R. Iyengar (1997): Visco-plastic analysis of adhesively bonded joints in composite materials, Advanced Composite Materials, 6:2, 99-121

To link to this article: http://dx.doi.org/10.1163/156855197X00021

Adv. Composite Mater., Vol. 6, No. 2, pp. 99–121 (1997)

Visco-plastic analysis of adhesively bonded joints in composite materials

S. C. PRADHAN,[1] N. N. KISHORE[2] and N. G. R. IYENGAR[3]

[1]*Structural Sciences Division, National Aerospace Laboratories, Bangalore 560 017, India*
[2]*Mechanical Engineering Department, Indian Institute of Technology, Kanpur 208 016, India*
[3]*Aerospace Engineering Department, Indian Institute of Technology, Kanpur 208 016, India*

Received 15 May 1995; accepted 15 April 1996

Abstract—Adhesively bonded joints are being preferred to mechanical fasteners in structural members because of distinct advantages they offer, such as uniform stress distribution, stiff connection, excellent fatigue properties and light weight. In addition, these joints are found to be more suitable with composite materials, particularly in the case of fibre reinforced plastics. At moderately large loads the polymeric adhesive material behaviour tends to elasto-plastic and elasto-visco-plastic. In the present work, a finite element code is developed and visco-plastic analyses of adhesively bonded joints are carried out. Single lap, stepped lap, and double lap joints are considered for the analyses. Influences of various parameters, such as (i) stacking sequence in composite adherends, (ii) critical strain energy release rate of the adhesive, (iii) overlap length and (iv) thickness of the adhesive on the strength of the adhesively bonded double lap joints, are also investigated.

Keywords: adhesive; composites; visco-plastic; FEM; strain energy release rate.

NOTATION

$\hat{a}$	flow vector
B_0	elastic strain displacement matrix
B_{NL}	strain displacement matrix, non-linear component
B^n	strain displacement matrix for nth iteration
C_0	prescribed constant
C^n	matrix
D	elastic constitutive relations
D_{vp}	visco-plastic constitutive relations
E	Young's modulus
F	flow rule expression
f^{n+1}	nodal forces of $(n+1)$th iteration

G_C	critical strain energy release rate of standard adhesive (epoxy)
G_I, G_{II}	strain energy release rates in modes I and II
G_{IC}, G_{IIC}	critical strain energy release rates in modes I and II
G'_C	assumed critical strain energy release rate of adhesive used
G_{xy}	shear modulus
g	G'_C/G_C
H	proportionality constant
H^n	matrix
J	J integral
J'_2	second invariant of deviatoric stresses
K_{IC}	stress intensity factor
K^n	stiffness matrix in nth iteration
L_o	overlap length
L_t	total length
l	L_o/L_t
M, N	prescribed constants
t	t_s/t_r
t_1	time in seconds in first iteration
t_n	time in seconds in nth iteration
t_r	thickness of the adherend
t_s	thickness of the adhesive
γ	fluidity parameter
γ_{xy}	fluidity parameter in pure shear mode
Δf^n	change in load during time interval Δt_n
Δt_n	incremental time in seconds in nth iteration
δ_{ij}	Kronecker delta
δ^n	displacement vector of nth iteration
ε_{ve}	visco-elastic strain
$\dot{\varepsilon}_{ss}$	steady state strain rate
$\dot{\varepsilon}_{ve}$	visco-elastic strain rate
$\dot{\varepsilon}_{vp}$	visco-plastic strain rate
$\dot{\varepsilon}_{vep}$	visco-elasto-plastic strain rate
Θ	prescribed constant
ν	Poisson's ratio
$\bar{\sigma}$	effective stress
σ_0	yield stress
σ_R	residual stress
σ'_{ij}	deviatoric stress components

σ_x, σ_y	normal stresses
τ_0	yield stress in pure shear mode
τ_{xy}	shear stress
Φ	function controlling visco-plastic flow rate
Ω	volume

1. INTRODUCTION

With the development of various structural adhesives, these joints are being employed in a wide variety of structural applications ranging from aerospace and automobile components to those found in microelectronic components. Adhesive are mostly polymeric materials and their responses are generally time dependent. Groth [1] concluded that events like moisture diffusion and delayed failure should be taken into account for an accurate analysis of adhesively bonded joints. At high stress levels, the non-linear visco-plastic effects could include creep strains as well. These would lead to significantly different results from the linear elastic predictions and therefore it is important that these effects are included. With the increase in load level, adhesive layers tend to become visco-plastic earlier than the adherends. Therefore, in the present analysis, only visco-plastic behaviour of adhesive is considered, while adherends are considered to be still within linear elastic range. Further, most of the finite element works, in the literature, have modelled the adhesive as a single layer of elements. In view of the significant difference in the stiffnesses of the adhesive and adherend, in the present work the adhesive is modelled as multi-layers of finite elements.

2. FORMULATION

Biot [2] derived the relevant equations to represent visco-elastic and relaxation responses by employing potential and dissipation functions. A large number of phenomena involving interaction of diffusion, chemical reaction, heat transfer and mechanical deformation are included in this theory. Zienkiewicz and Cormeau [3] developed an elasto-visco-plastic algorithm, which is found to be an efficient tool and is applicable to a wide range of non-linear (material) problems. The solution technique developed is capable of handling visco-elastic and visco-plastic effects, and various combinations of them. However, the most efficient way of dealing with large deformation and dynamic effects is not resolved. Zienkiewicz *et al.* [4] discussed the finite element method of solution of elasto-visco-plastic engineering problems. For computation convenience, bulk material is considered to be composed of several layers, where each layer might have different material characteristics. However, this model was limited to isotropic materials and includes very few material laws. Kanchi *et al.* [5] discussed a visco-plastic technique and employed this to study the problems of plastic and creep instability. Schapery [6] discussed pertinent aspects of the J integral and energy release rate theory for non-linear elastic media. He developed methods

of quasi-static deformation and fracture analysis for non-linear visco-elastic media. The corresponding principles, which provide the basis for the analysis are applicable to crack growth, crack closure and other problems such as ablation and interfacial contact and separation.

2.1. *Strain rate* (Reference [7])

Groth [8] presented expression for visco-elastic, visco-plastic and visco-clasto-plastic strain rate as given in equations (1)–(5) for the one-dimensional models of adhesive material under pure shear, as shown in Fig. 1.

$$\dot{\varepsilon}_{ve} = \gamma_{xy}[\tau_{xy} - G_{xy}\varepsilon_{ve}], \tag{1}$$

$$\dot{\varepsilon}_{vp} = \gamma_{xy}[\tau_{xy} - \tau_0] \quad \text{if} \quad \tau_{xy} > \tau_0 \tag{2}$$

$$= 0 \qquad\qquad \text{if} \quad \tau_{xy} \leqslant \tau_0, \tag{3}$$

$$\dot{\varepsilon}_{vep} = \gamma_{xy}[\tau_{xy} - G_{xy}\varepsilon_{ve}] + \gamma_{xy}[\tau_{xy} - \tau_0] \quad \text{if} \quad \tau_{xy} > \tau_0 \tag{4}$$

$$= \gamma_{xy}[\tau_{xy} - G_{xy}\varepsilon_{ve}] \qquad \text{if} \quad \tau_{xy} \leqslant \tau_0. \tag{5}$$

From the equations, (2) and (4), it is observed that the expressions for strain rates are different for different adhesive models. Visco-plastic strain rate $\dot{\varepsilon}_{vp}$ for two-dimensional analysis is expressed as

$$\dot{\varepsilon}_{vp} = \gamma\langle\Phi\rangle\hat{a}, \tag{6}$$

where γ, Φ and $\hat{a}$ are fluidity parameter, visco-plastic flow function and flow vector, respectively. $\langle\Phi\rangle$ indicates positive values of Φ. Fluidity parameter, γ, is a material constant. Different expressions are recommended for the function Φ by Owen and

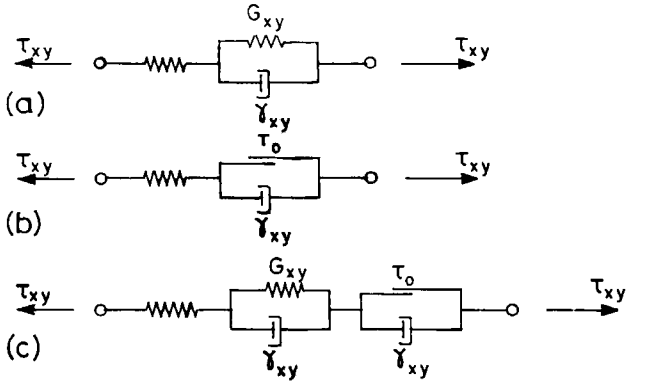

Figure 1. Adhesive material models: (a) the three parameter solid model, (b) the Bingham visco-plastic model, and (c) the five parameter visco-elastic–visco-plastic model.

Hinton [7] and by Zienkiewicz and Taylor [9]. The most common representations are

$$\Phi = e^M\left(\frac{F-\sigma_0}{\sigma_0}\right) - 1, \tag{7}$$

$$\Phi = \left(\frac{F-\sigma_0}{\sigma_0}\right)^N, \tag{8}$$

$$\Phi = \frac{F}{\sigma_0}, \tag{9}$$

where M and N are material constants and σ_0 is yield stress. Flow rule, F, associated with these equations is assumed as

$$F = \sqrt{\sigma_x^2 + \sigma_y^2 - \sigma_x\sigma_y + 3\tau_{xy}^2}. \tag{10}$$

Flow vector ($\hat{a}$) is given as

$$\hat{a} = \frac{\sqrt{3}}{2J_2'}\begin{Bmatrix} \sigma_x' \\ \sigma_y' \\ 2\tau_{xy}' \end{Bmatrix}. \tag{11}$$

Deviatoric stress components are denoted by primes and these are obtained from

$$\sigma_{ij}' = \sigma_{ij} - \frac{\delta_{ij}\sigma_{kk}}{3}. \tag{12}$$

J_2' represents the second invariants of deviatoric stresses and is written as

$$J_2' = \frac{1}{2}\left(\sigma_x'\sigma_x' + \sigma_y'\sigma_y'\right) + \tau_{xy}^2. \tag{13}$$

2.2. Visco-plastic constitutive relation (Reference [7])

The visco-plastic stress-strain relation is written as

$$D_{\text{vp}} = \left[D^{-1} + C^n\right]^{-1}. \tag{14}$$

D is the material matrix of linear elastic material and C^n is given as

$$C^n = \Theta\Delta t_n H^n, \tag{15}$$

where Θ is a constant, Δt_n is the incremental time of nth interval and H^n is given as

$$H^n = p_1 m_1 + p_2 m_2, \tag{16}$$

where p_1, p_2, m_1 and m_2 are expressed as

$$p_1 = \gamma \left\langle \frac{\sqrt{3}}{2(J_2')^{1/2}} \Phi \right\rangle, \tag{17}$$

$$p_2 = \gamma \left\langle \frac{\sqrt{3}}{4(J_2')} \frac{\mathrm{d}\Phi}{\mathrm{d}F} - \frac{\sqrt{3}\Phi}{4(J_2')^{3/2}} \right\rangle, \tag{18}$$

$$m_1 = \begin{bmatrix} 2/3 & -1/3 & 0 \\ -1/3 & 2/3 & 0 \\ 0 & 0 & 2 \end{bmatrix}, \tag{19}$$

$$m_2 = \begin{bmatrix} \sigma_x'\sigma_x' & \sigma_x'\sigma_y' & 2\sigma_x'\tau_{xy} \\ \sigma_x'\sigma_y' & \sigma_y'\sigma_y' & 2\sigma_y'\tau_{xy} \\ 2\sigma_x'\tau_{xy} & 2\sigma_y'\tau_{xy} & 4\tau_{xy}^2 \end{bmatrix}. \tag{20}$$

2.3. *Finite element algorithm*

A computer program similar to the one developed by Owen and Hinton [7], is developed to predict the failure loads of adhesive joints. The corresponding flow chart is illustrated in Fig. 2. The module, which takes into account the non-linear visco-plastic behaviour of the material is indicated by the dashed portion in the flow chart. Details of the main algorithm are given in [10].

The additional visco-plastic part of the algorithm developed is explained as follows:

step 1: at time $t = t_n$ find the following:

$$B^n = B_0 + B_{\mathrm{NL}}\delta^n,$$
$$C^n = C^n(\sigma^n,\ \Delta t_n),$$
$$D_{\mathrm{vp}}^n = [D^{-1} + C^n]^{-1},$$
$$K_{\mathrm{T}}^n = \int_{\Omega} [B^n]^{\mathrm{T}} D_{\mathrm{vp}}^n B^n \mathrm{d}\Omega,$$
$$\dot{\varepsilon}_{\mathrm{vp}}^n = \gamma \langle \Phi \rangle \hat{a}^n.$$

step 2: compute incremental displacements and stresses:

$$(\text{if } t = t_1 \text{ calc. } \Delta\psi_{\mathrm{vp}}^n = \int_{\Omega} [B^n]^{\mathrm{T}} D_{\mathrm{vp}}^n \dot{\varepsilon}_{\mathrm{vp}}^n \Delta t_n \mathrm{d}\Omega + \Delta f^n),$$
$$\Delta\delta^n = [K_{\mathrm{T}}^n]^{-1} \Delta\psi_{\mathrm{vp}}^n,$$
$$\Delta\sigma^n = D_{\mathrm{vp}}(B^n \Delta\delta^n - \dot{\varepsilon}_{\mathrm{vp}}^n \Delta t^n).$$

step 3: update displacements and stresses:

$$\delta^{n+1} = \delta^n + C_0 \Delta\delta^n,$$
$$\sigma^{n+1} = \sigma^n + \Delta\sigma^n,$$

where C_0 is a constant multiplier used for fast convergence.

step 4: calculate visco-plastic strain:

$$\dot{\varepsilon}_{\mathrm{vp}}^{n+1} = \gamma \langle \Phi \rangle \hat{a}^{n+1}.$$

step 5: calculate proportionality factor H:

$$H = \frac{\sigma^{n+1} - \sigma^{n}}{\sigma_0 - \sigma^{n}}.$$

step 6: compute residual stress to be compensated:

$$\sigma_{\mathrm{R}} = H\sigma^{n+1}.$$

step 7: update stress:

$$\sigma^{n+1} = (1 - H)\sigma^{n+1},$$

where σ_{R} represents the residual stress.

step 8: apply equilibrium correction:

$$\Delta\psi_{\mathrm{vp}}^{n+1} = \int_{\Omega} [B^{n+1}]^{\mathrm{T}} D_{\mathrm{vp}}^{n+1} \dot{\varepsilon}_{\mathrm{vp}}^{n+1} \Delta t_{n+1} \mathrm{d}\Omega + \Delta f^{n+1} + \psi^{n+1},$$

$$\psi^{n+1} = \int_{\Omega} [B^{n+1}]^{\mathrm{T}} \sigma_{\mathrm{R}}^{n+1} \mathrm{d}\Omega + f^{n+1},$$

where f^{n+1} represents nodal forces.

step 9: check if visco-plastic strain rate is close to steady state value:

$|\dot{\varepsilon}_{\mathrm{vp}}^{n+1}| \leqslant \dot{\varepsilon}_{\mathrm{ss}}$ i.e. tolerance

if steady state is reached go to *main algorithm*, or else go to step 1.

B^n, σ^n, D_{vp}^n, K^n and $\dot{\varepsilon}_{\mathrm{vp}}^n$ represent strain displacement matrix, stress tensor, visco-plastic stress–strain relation, stiffness matrix and visco-plastic strain rate, respectively of nth iteration. B^n, σ^n, C^n, D_{vp}, and K^n are functions of the displacement vector of nth iteration. These values are updated in every iteration. However, there is a possibility of divergence in the results by using the K^n values. Using constant values of B^n and K^n and Newton–Raphson's modified approximation (Owen and Hinton [7] and Zienkiewicz and Taylor [9]) one can achieve convergence. Further, this reduces substantially the computational time and memory. However, $\dot{\varepsilon}_{\mathrm{vp}}^n$ and D_{vp}^n are updated in each time step.

If the effective stress $\bar{\sigma}$ of any element in the adhesive exceeds the yield value of the material σ_0, then the material state becomes visco-plastic and therefore visco-plastic analysis is carried out. Visco-plastic module of elasto-visco-plastic analysis is indicated by the dashed box of Fig. 2.

Visco-plastic calculations are repeated until the strain rate has reached a steady state value ($\dot{\varepsilon}_{\mathrm{ss}}$). Then strain energy release rates are calculated by the technique discussed in [10]. The fracture criterion $G_{\mathrm{I}} + G_{\mathrm{II}} \geqslant G_{\mathrm{IC}} + G_{\mathrm{IIC}}$ is employed to predict the failure loads.

The developed code is quite general, and could be employed for visco-elastic, visco-plastic and elasto-visco-plastic analysis of adhesive materials. All that one needs is to incorporate the corresponding behaviour of the models for adhesives in the expression for strain rate.

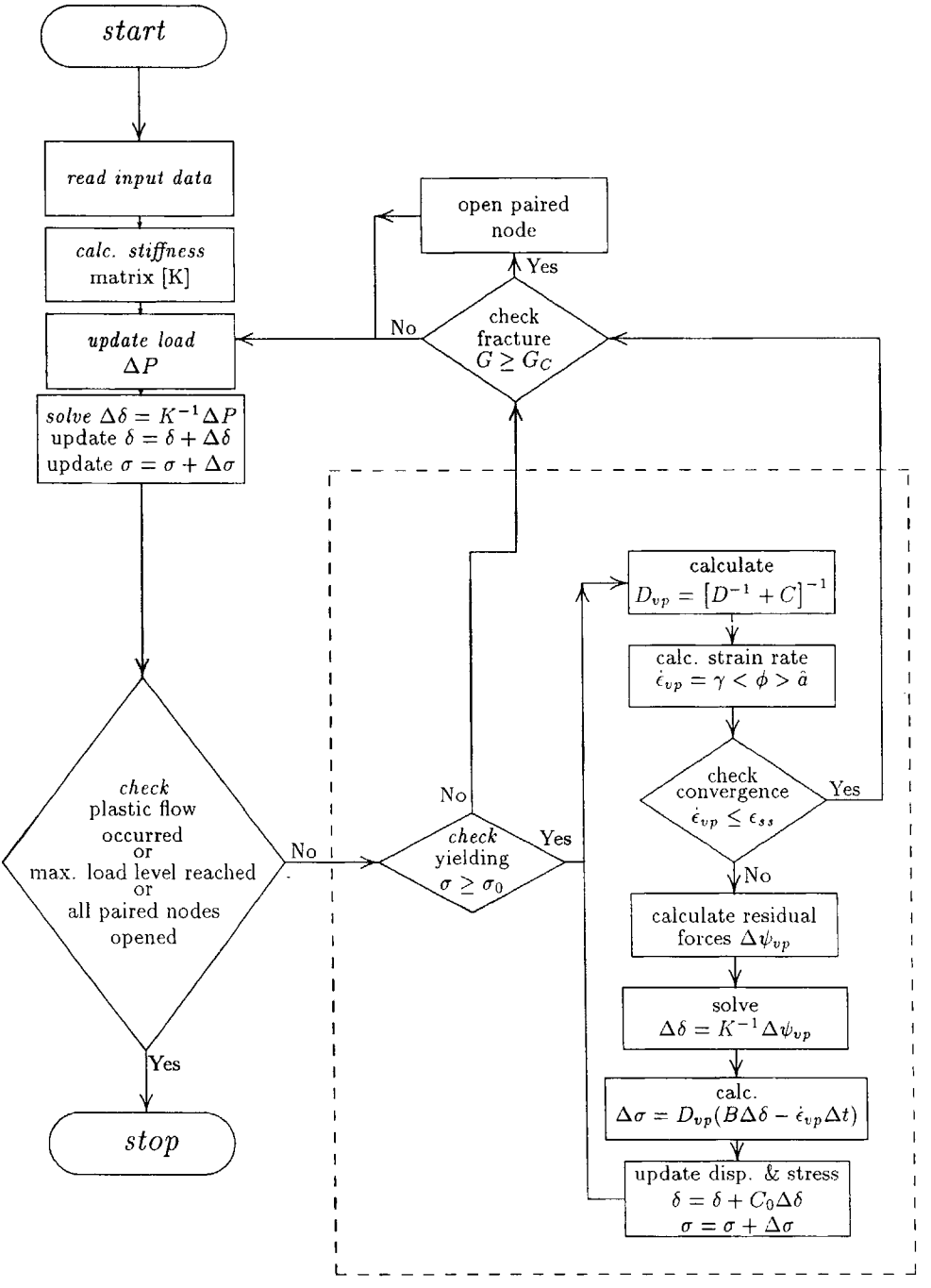

Figure 2. Flow chart of visco-plastic finite element analysis.

3. RESULTS AND DISCUSSION

3.1. Validation

In order to validate the developed computer code, the two-dimensional visco-plastic perforated plate problem analysed by Zienkiewicz *et al.* [4] is considered. A schematic diagram of this plate is shown in Fig. 3. The physical dimensions and the material properties of the plate are listed in Table 1. The stress level is plotted in Fig. 4 against

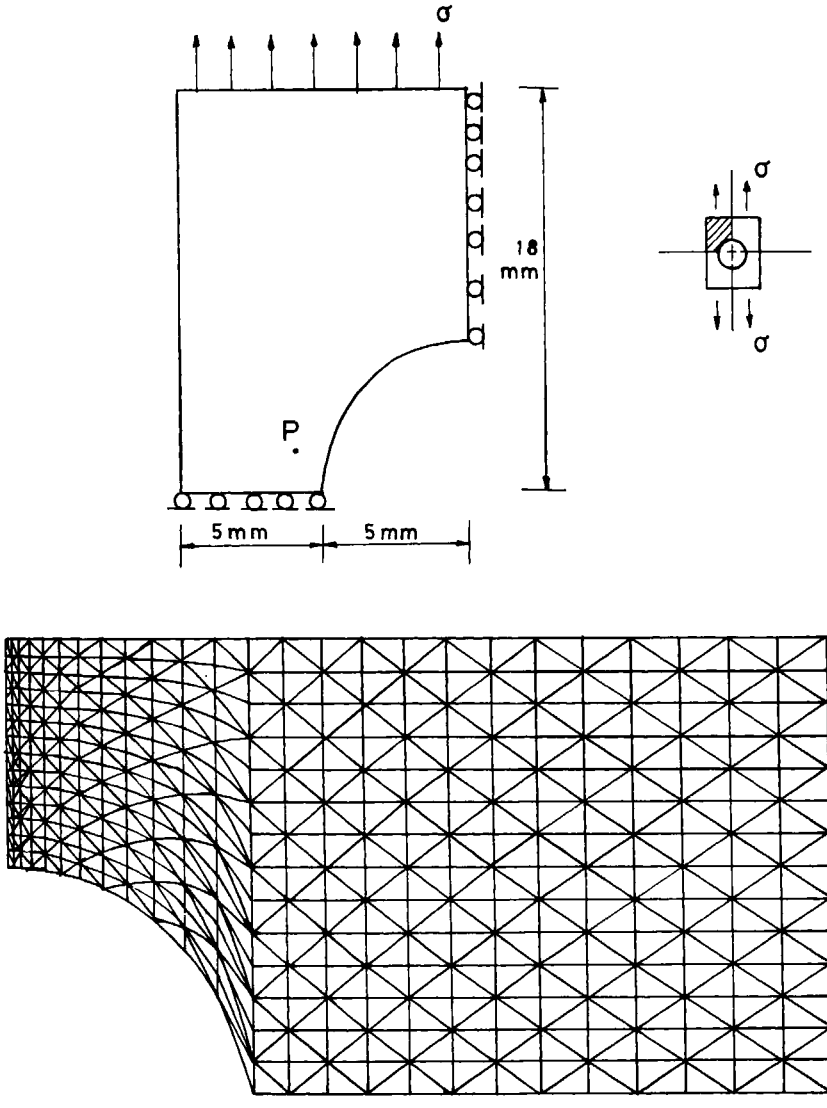

Figure 3. Schematic of perforated plate under uniform tension (Zienkiewicz *et al.* [4]) showing the plastic element $\mathcal{P}$ and the finite element mesh of the plate.

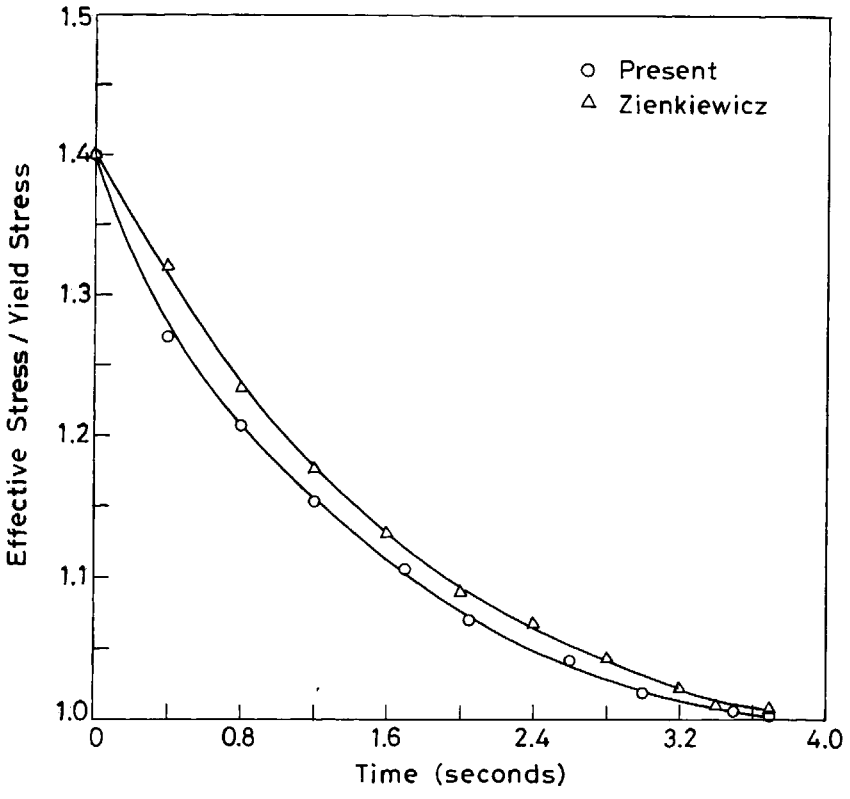

Figure 4. Variation of stress with time for plastic element $\mathcal{P}$ of the perforated plate (Fig. 3).

Table 1.
Specifications of the perforated plate problem (Zienkiewicz *et al.* [4])

	Perforated plate
Dimension of plate	36 mm × 20 mm
Diameter of the circular cut out	10 mm
Young's modulus (E)	70 GPa
Poisson's ratio (ν)	0.2
Stress applied (σ)	95 MPa
Yield stress σ_0	243 MPa
Fluidity parameter (γ)	0.01 s^{-1}

the time for an element $\mathcal{P}$, which is in the plastic range. The results is in fairly good agreement with that by Zienkiewicz *et al.* [4].

3.2. Single lap joint

Using the developed finite element code elastic and visco-plastic analyses are carried for a single lap joint (Hiregoudar [11]). Details of the joint (Fig. 5) are shown

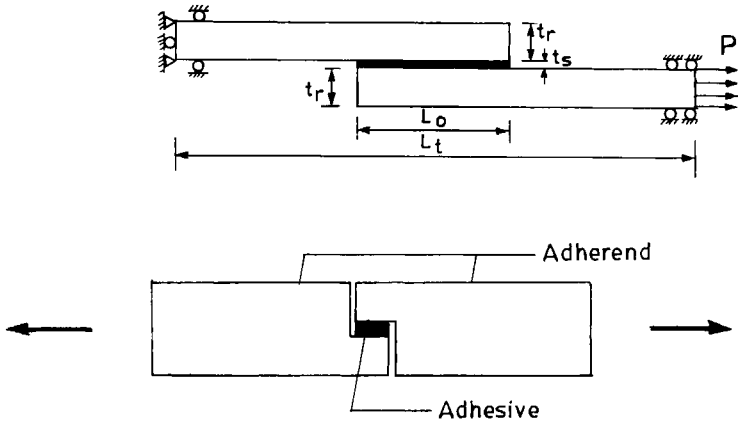

Figure 5. Schematic of single and step lap joints.

Table 2.
Specifications of single lap joint (Hiregoudar [11])

Single lap joint	
Overlap length (L_o)	16 mm
Total length (L_t)	80 mm
Applied stress (σ)	200 MPa
Adhesive thickness (t_s)	0.30 mm
Adherend thickness (t_r)	1.60 mm
Adhesive (FM 73)	
Young's modulus (E_s)	2.21
Poisson's ratio (ν_s)	0.43
Yield stress σ_0	40 MPa
Fluidity parameter (γ)	4.495×10^{-3} s^{-1}
Constant N	1.426
Constant Θ	1.4
Flow functions (Φ)	$\left(\frac{F-\sigma_0}{\sigma_0}\right)^N$
Adherend (Steel)	
Young's modulus (E_r)	211.3 GPa
Poisson's ratio (ν_s)	0.33
Yield stress σ_0	∞

in Table 2. Stresses along the overlap length of the single lap joint are computed from elastic and visco-plastic analyses and these results are compared in Fig. 6. The maximum difference in the computed peel stress along the overlap length of the single lap joint is less than 3.6 per cent, while this difference for shear stress is less than 11.4 per cent. Peel stresses predicted by the present analysis and visco-plastic analysis carried out by Hiregoudar [11] are also compared in Fig. 7. The difference in the computed peel stress along the overlap length of the single lap joint is less than 11 per cent. It is also observed that this difference is maximum near the edges and gradually reduces to a minimum towards the central part of the overlap.

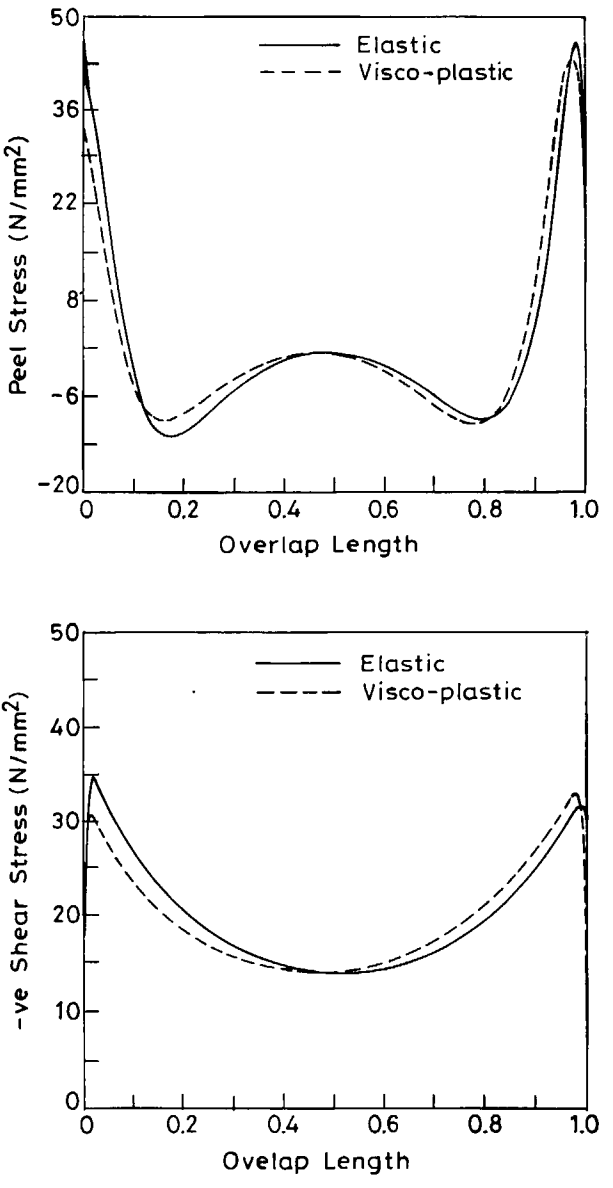

Figure 6. Comparison of elastic and visco-plastic stress distribution along the overlap length of single lap joint (Hiregoudar [11]).

Using the present finite element code the result obtained for the visco-plastic analysis of the perforated plate problem of Zienkiewicz *et al.* [4] is in good agreement with that reported by Zienkiewicz *et al.*, while Hiregoudar [11] has developed has finite element code for the visco-plastic analysis but has not validated his computer code with any standard bench mark problem.

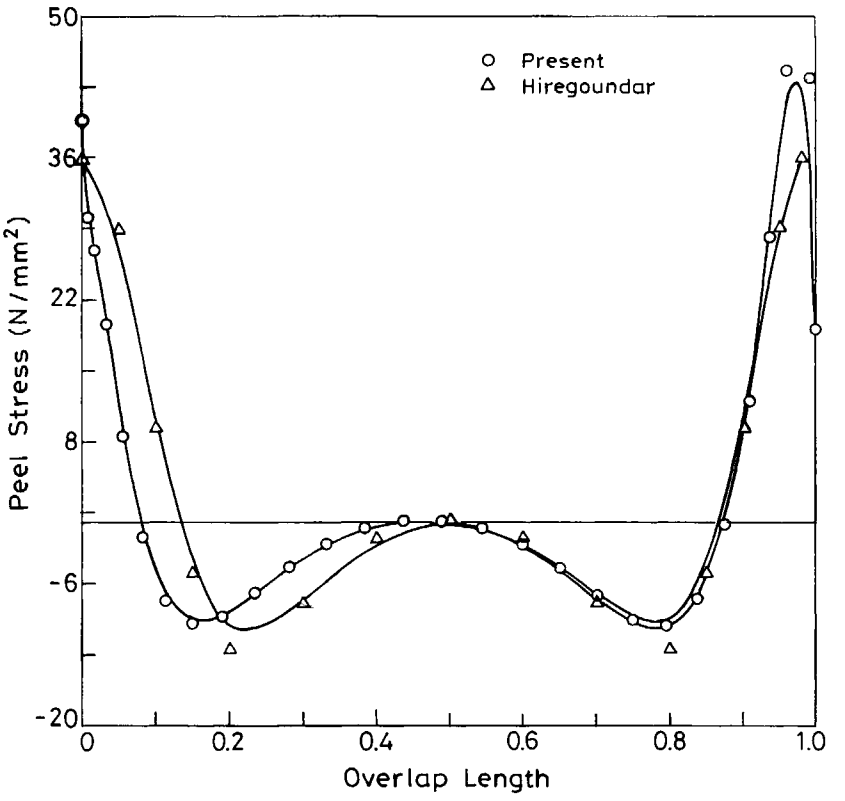

Figure 7. Comparison of peel stress distribution along the overlap length of single lap joint (Hiregoudar [11]).

In the present analysis a refined mesh consisting of 1816 constant strain triangle (CST) elements is used, while Hiregoudar [11] has employed a course mesh consisting of 300 elements. Further in the present analysis the adhesive is modelled as six layers of elements, while it is modelled as a single layer of elements by Hiregoudar [11]. Detail of mesh refinement of the bonded joints and its effect on fracture parameters are discussed in [12]. However, we feel that our results are more accurate as compared to those of Hiregoudar [11], in view of the use of a validated visco-plastic finite element code and refined mesh near the edges in the finite element model of the bonded joints.

3.3. Stepped lap joint

Using the present finite element code, visco-plastic analysis is carried out for the stepped lap joint (Su and Mackie [13]). The joint (Fig. 5) specifications are listed in Table 3. Visco-plastic parameters such as fluidity parameter (γ), material constants (N, Θ) and flow function (Φ) of the epoxy adhesive are considered to be as those of epoxy adhesive (FM73). In Fig. 8 the shear stress and shear strain distributions, in the adhesive along the overlap and near the interface of adherend and adhesive, are

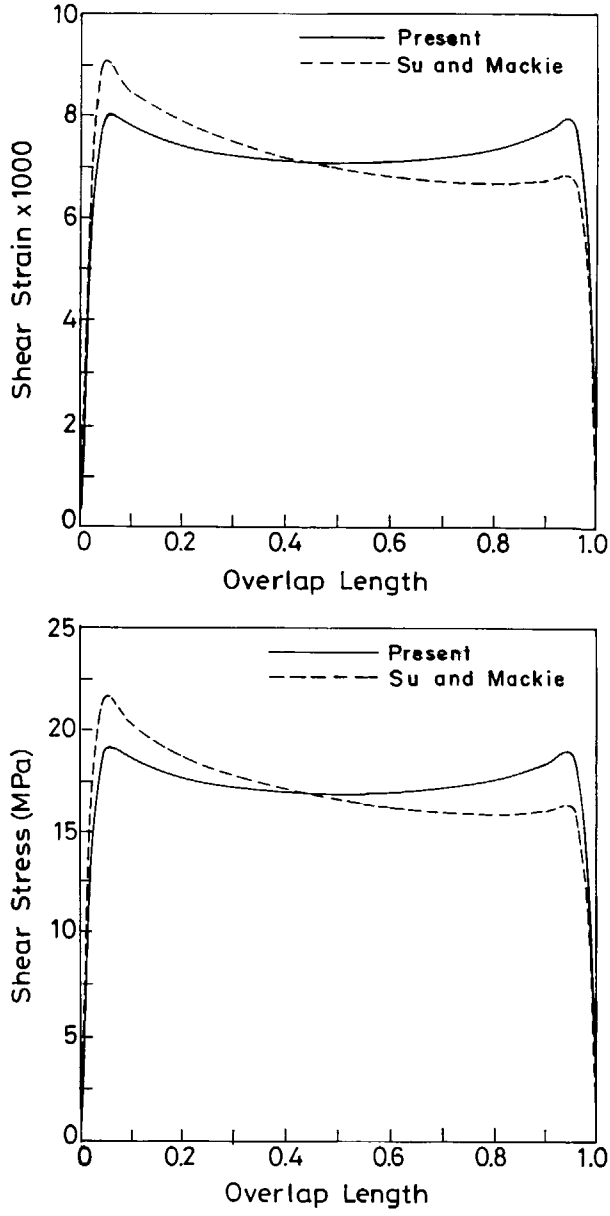

Figure 8. Comparison of shear stress and strain distribution along the overlap length at interface of adherend and adhesive of the stepped lap joint.

compared with those of Su and Mackie [13]. The difference is found to be less than 11.7 per cent. It is also observed that this difference is maximum near the edges and gradually reduces to a minimum towards the central part of the overlap length. In the present analysis a refined mesh consisting of 1816 CST elements is used, while Su and Mackie [13] have employed a course mesh consisting of nearly 100 elements.

Table 3.
Specifications of stepped lap joint (thick adherend shear test specimen) of Su and Mackie [13]

Joint configuration	
Overlap length (L_o)	8 mm
Total length (L_t)	125 mm
Applied stress (P)	3.5 kN
Total joint thickness (t)	13.35 mm
Width of the joint (W)	25.4 mm
Adhesive (rubber-toughened epoxy)	
Young's modulus (E_s)	6.60 GPa
Poisson's ratio (ν_s)	0.38
Thickness of adhesive (t_s)	0.65 mm
Yield stress (σ_0)	50 MPa
Fluidity parameter (γ)	4.495×10^{-3} s^{-1}
Constant N	1.426
Constant Θ	1.4
Flow function (Φ)	$\left(\frac{F-\sigma_0}{\sigma_0}\right)^N$
Adherend (Steel)	
Young's modulus (E_r)	210 GPa
Poisson's ratio (ν_r)	0.3
Thickness of adherend (t_r)	6.35 mm

Further in the present analysis the adhesive is modelled as six layers of elements, while it is modelled as a single layer of elements by Su and Mackie [13]. Because of the use of refined mesh near the edges as compared to Su and Mackie [13], the present results are expected to be accurate.

3.4. Double lap joint

Effects of crack location, stacking sequence, critical strain energy release rate of adhesive material, overlap length and adhesive thickness on the strength of double lap joint (Fig. 9) are investigated. Because of symmetry, only one half of the joint is considered for the analysis. The problem is treated as one of plane strain and a finite element mesh consisting of 1816 CST elements is employed for the analysis.

Three non-dimensional parameters are defined, namely,

$$\mathbf{g} = \frac{G'_C}{G_C}, \tag{21}$$

$$\mathbf{l} = \frac{L_o}{L_t}, \tag{22}$$

$$\mathbf{t} = \frac{t_s}{t_r}, \tag{23}$$

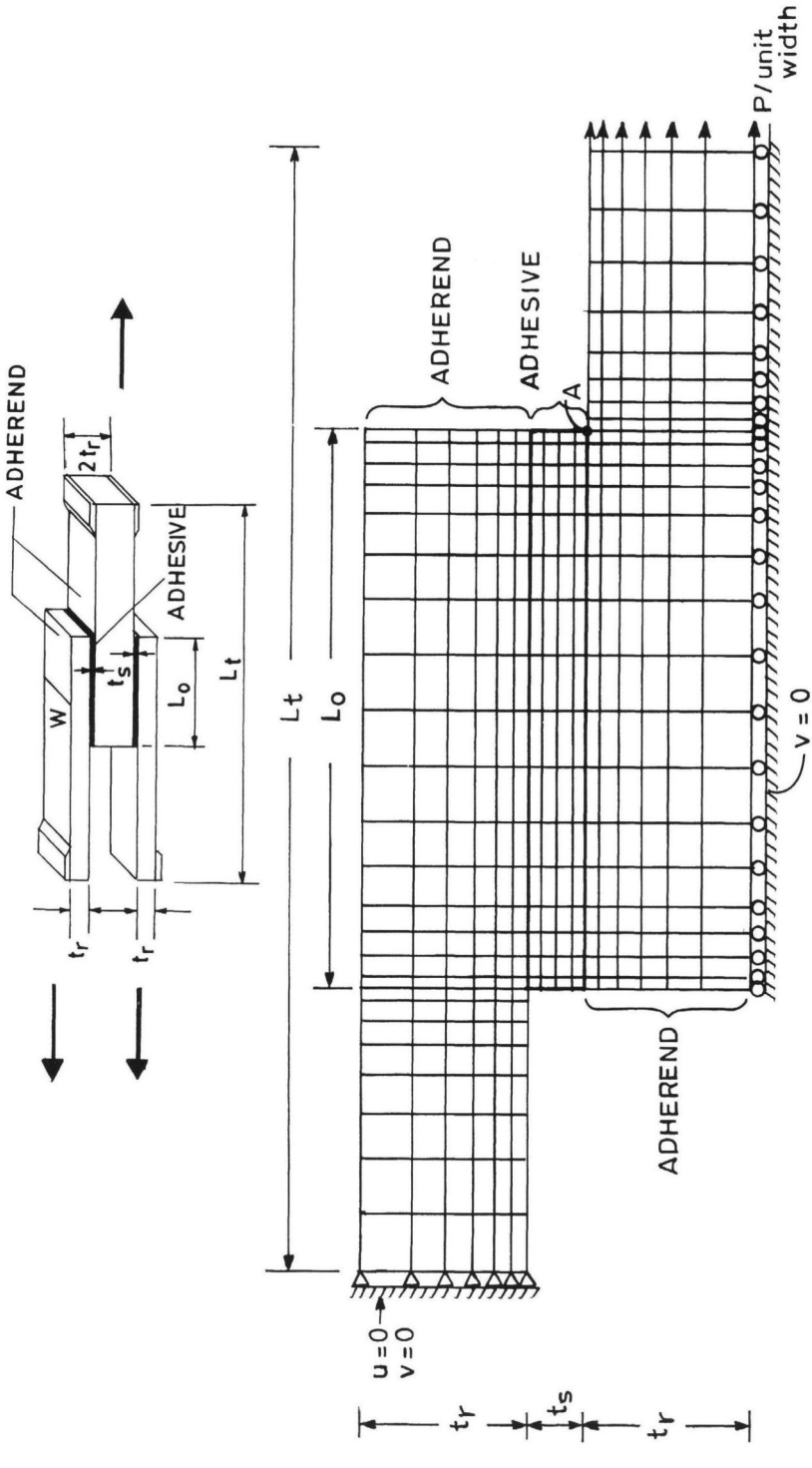

Figure 9. Schematic of adhesively bonded double lap joint and the finite element mesh showing the crack location 'A'.

Table 4.
Specifications of double lap joint

Double lap joint	
Overlap length (L_o)	40 mm
Total length (L_t)	80 mm
Adherend (carbon fibre reinforced plastic)	
Longitudinal modulus (E_l)	137 GPa
Transverse modulus (E_t)	7 GPa
Shear modulus (G_{lt})	4.5 GPa
Poisson's Ratio (ν_{lt})	0.3
Adherend thickness (t_r)	10 mm
Adhesive (Epon VIII)	
Young's modulus (E_s)	3.5 GPa
Poisson's ratio (ν_s)	0.41
Thickness of adherend (t_s)	2 mm
Fracture toughness (G_C)	0.36 kJ/m^2
Yield stress σ_0	45 MPa
Fluidity parameter (γ)	4.495×10^{-3} s^{-1}
Constant N	1.426
Constant Θ	1.4
Flow functions (Φ)	$\left(\frac{F-\sigma_0}{\sigma_0}\right)^N$
Fracture criterion $G_I + G_{II} \geqslant G_C$	

where G'_C and G_C are the fracture toughnesses of the adhesive employed and the standard adhesive (epoxy), respectively. L_o and L_t denote the overlap length and the total length of the bonded joint. In addition t_s and t_r represent the thicknesses of adhesive and adherend, respectively. G'_C is considered to be in multiples of G_C. Assuming constant fracture toughness of the adhesive (G_C), adherend thickness t_r and overlap length L_o parametric study is carried out. The adherends and adhesive of the joint are considered to be carbon fibre reinforced plastics (CFRP) and Epon VIII (Table 4), respectively. Visco-plastic parameters such as fluidity parameter (γ), material constants (N, Θ) and flow function (Φ) of the epoxy adhesive (Epon VIII) are considered to be as those of epoxy adhesive (FM73). Critical crack location 'A' is considered in the present work.

3.4.1. Stacking sequence. Symmetric quasi-isotropic combinations are considered to investigate the effect of stacking sequence on the bond strength. Four fibre orientations considered are 0°, 45°, 90° and −45°. In an earlier work [10], it was found $[0°/45°/90°/-45°]_S$ laminate exhibits maximum bond strength. Further, the presence of 0° ply in the immediate neighbourhood of the adhesive results in stronger joint. Visco-plastic analysis is carried out for three different layup sequences, namely, $[0°/0°/0°/0°]_S$, $[0°/45°/90°/-45°]_S$ and $[0°/0°/90°/90°]_S$ of CFRP adherends. It is found that $[0°/0°/90°/90°]_S$ layup is stronger than $[0°/45°/90°/-45°]_S$ layup. The failures loads are compute for various adhesive fracture toughnesses ratio

Table 5.
Computed failure loads for various $\mathbf{g}(= G'_C/G_C)$ values and different laminae combinations

G'_C/G_C	Crack length (mm)	Failure loads in N/mm for $L_o/L_t = 0.50$ and $t_s/t_r = 0.20$ $[0°/0°/0°/0°]_S$	$[0°/0°/90°/90°]_S$	$[0°/45°/90°/-45°]_S$
0.1	0.164	5.760	5.984	5.696
0.2	0.164	8.096	8.416	8.032
0.3	0.164	9.920	10.304	9.856
0.4	0.164	11.520	11.904	11.392
0.5	0.164	12.800	13.312	12.672
0.6	0.164	14.080	14.592	14.016
0.7	0.164	15.232	15.872	15.168
0.8	0.164	16.384	17.024	25.472
0.9	0.164	17.472	18.304	16.192
1.0	0.164	18.560	19.456	17.408
1.1	0.164	19.840	20.736	18.944
1.2	0.164	20.992	22.016	20.096
1.3	0.164	22.400	23.296	21.632
1.4	0.164	23.552	24.576	23.040
1.5	0.164	24.704	25.984	24.320

$\mathbf{g}(= G'_C/G_C)$, overlap lengths $\mathbf{l}(= L_o/L_t)$ and adhesive thickness ration $\mathbf{t}(= t_s/t_r)$ for these three layups. Detail of these results are discussed in the respective sections.

3.4.2. Fracture toughness of adhesive. For various $\mathbf{g}(= G'_C/G_C)$ values and layups the computed failure loads are listed in Table 5. As was found in the linear elastic analysis reported in [10], in the present visco-plastic analysis also it is observed that as **g** increases, failure load increases for all the three layup sequences considered. Adhesives with higher critical strain energy release rate (high **g** value) lead to a stronger joint. Therefore, in order to achieve a higher fracture strength of the joint, adhesives with higher critical strain energy release rate are suggested. Only variation of failure load with crack length for various **g** values in $[0°/0°/0°/0°]_S$, $[0°/0°/90°/90°]_S$ and $[0°/45°/90°/-45°]_S$ (optimal) CFRP laminates are shown in Fig. 10.

Fracture toughness of adhesive is generally denoted by K_{IC}, the stress intensity factor for ideal plane strain adhesive material. In th present study, for convenience critical strain energy release rate G_C is termed as fracture toughness.

3.4.3. Overlap length. For various values of $\mathbf{l}(= L_o/L_t)$ and the three layups chosen, the computed failure loads are listed in Table 6. As was found in the linear elastic analysis reported in [10], in the present visco-plastic analysis also it is observed that as **l** increases, failure load increases for all the three layup sequences. For higher fracture strength of the bond, larger overlap length (high **l**) is suggested. Variation of failure load with crack length for various **l** values in $[0°/0°/0°/0°]_S$, $[0°/0°/90°/90°]_S$ and $[0°/45°/90°/-45°]_S$ (optimal) CFRP laminates are depicted in Fig. 11.

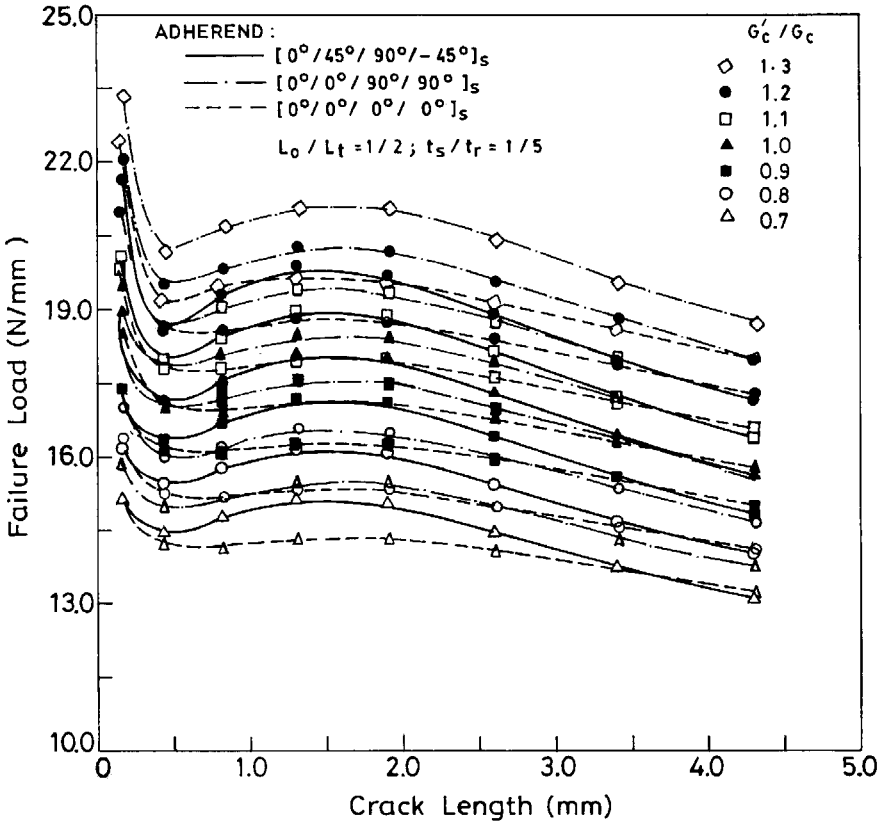

Figure 10. Variation of failure load with crack length for crack initiation at location 'A' and different $\mathbf{g}(= G'_C/G_C)$ values in $[0°/0°/0°/0°]_S$, $[0°/0°/90°/90°]_S$ and $[0°/45°/90°/-45°]_S$ (optimal) CFRP laminates.

Table 6.
Computed failure loads for various $\mathbf{l}(= L_o/L_t)$ values and different laminae combinations

L_o/L_t	Crack length (mm)	Failure loads in N/mm for $G'_C/G_C = 0.40$ and $t_s/t_r = 0.20$ $[0°/0°/0°/0°]_S$	$[0°/0°/90°/90°]_S$	$[0°/45°/90°/-45°]_S$
0.307	0.050	4.463	–	–
0.333	0.054	4.752	4.607	4.271
0.363	0.059	5.112	4.968	4.607
0.400	0.065	5.472	5.448	5.040
0.444	0.073	5.832	5.880	5.520
0.500	0.164	11.616	12.048	11.472

– plastic flow.

3.4.4. Adhesive thickness. For various $\mathbf{t}(= t_s/t_r)$ values and layups the computed failure loads are listed in Table 7. As was found in the linear elastic analysis reported in [10], in the present visco-plastic analysis also it is observed that as **t** increases,

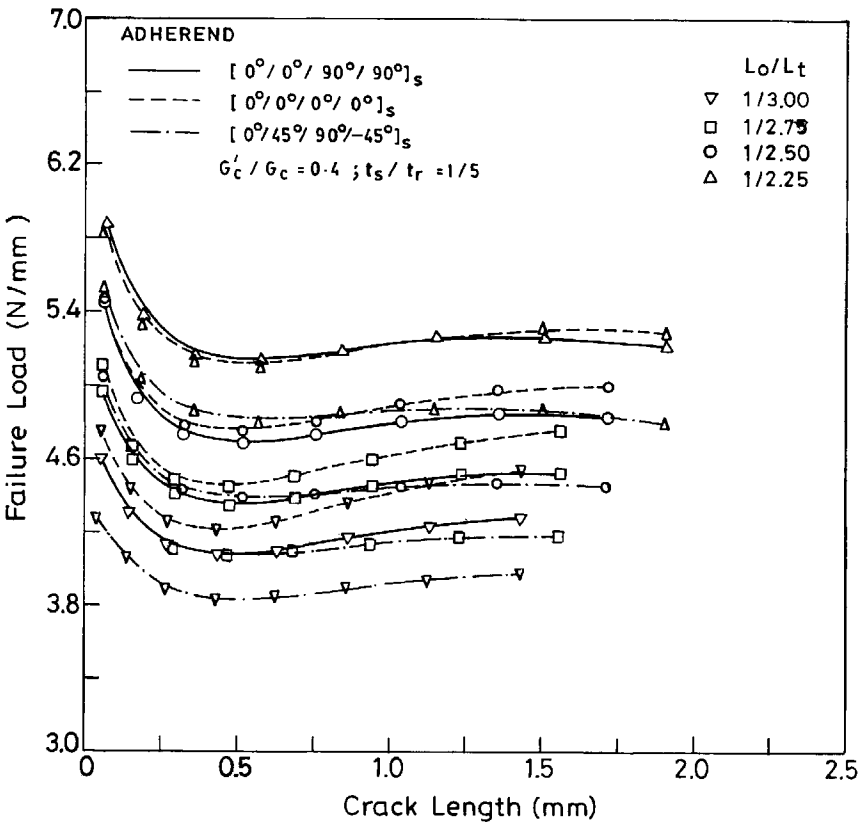

Figure 11. Variation of failure load with crack length for crack initiation at location 'A' and different $\mathbf{l}(= L_o/L_t)$ values in $[0°/0°/0°/0°]_S$, $[0°/0°/90°/90°]_S$ and $[0°/45°/90°/-45°]_S$ (optimal) CFRP laminates.

Table 7.
Computed failure loads for various $\mathbf{t}(= t_s/t_r)$ values and different laminae combinations

t_s/t_r	Crack length (mm)	Failure loads in N/mm for $G'_C/G_C = 0.40$ and $L_o/L_t = 0.50$ $[0°/0°/0°/0°]_S$	$[0°/0°/90°/90°]_S$	$[0°/45°/90°/-45°]_S$
0.012	0.164	16.384	17.792	16.128
0.025	0.164	15.488	16.000	14.848
0.033	0.164	15.040	15.296	14.528
0.050	0.164	14.336	14.592	13.696
0.100	0.164	13.056	13.440	12.672
0.200	0.164	11.616	12.048	11.472

failure load decreases for the three layup sequences. For higher fracture strength of the bond, small thickness of the adhesive (low **t**) is suggested. Variation of failure load with crack length for various **t** values in $[0°/0°/0°/0°]_S$, $[0°/0°/90°/90°]_S$ and $[0°/45°/90°/-45°]_S$ (optimal) CFRP laminates are shown in Fig. 12.

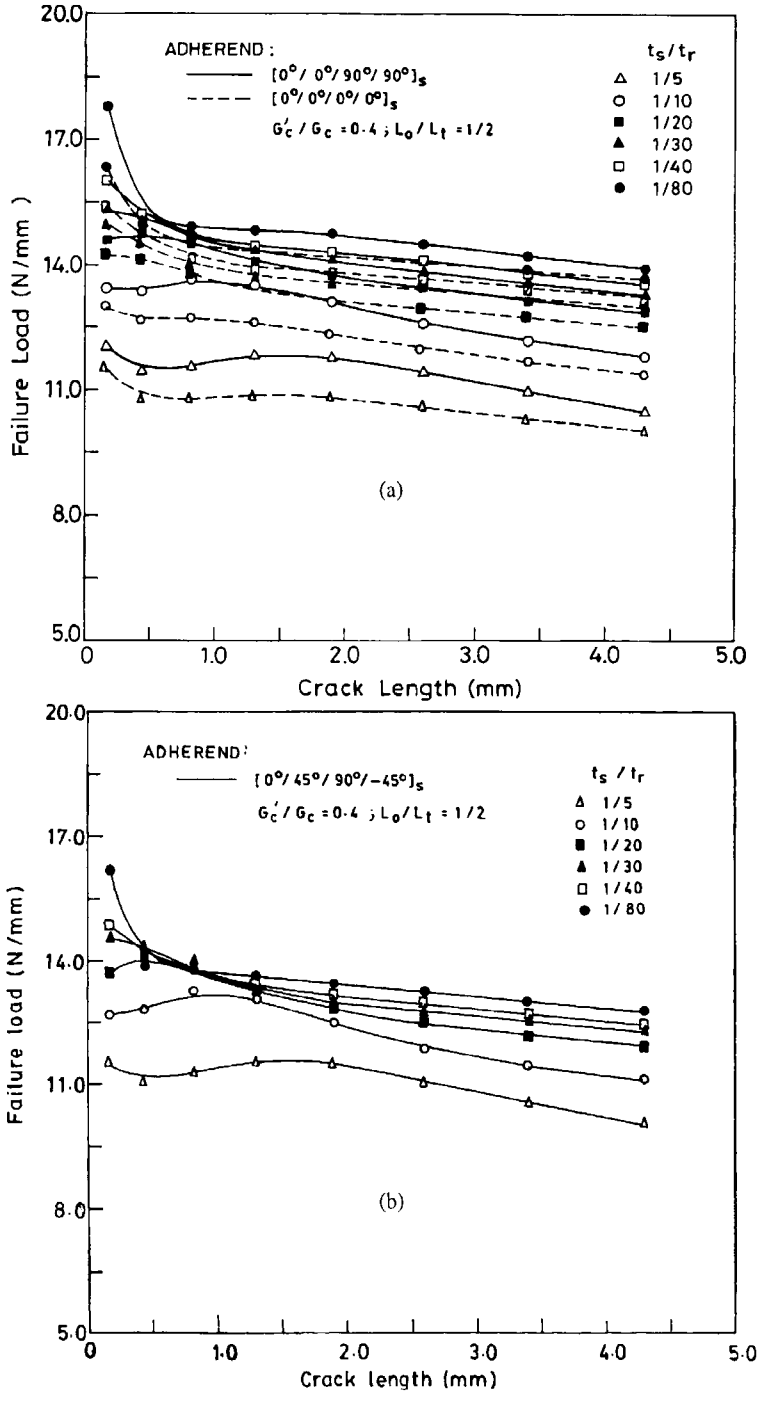

Figure 12. Variation of failure load with crack length for crack initiation at location 'A' and different $\mathbf{t}(=t_s/t_r)$ values in $[0°/0°/0°/0°]_S$, $[0°/0°/90°/90°]_S$ (a) and $[0°/45°/90°/-45°]_S$ (b) (optimal) CFRP laminates.

4. CONCLUSIONS

On the basis of elasto-visco-plastic analysis carried out, the following conclusions are drawn

- The elastic analysis predicts lower failure loads as compared to the elasto-visco-plastic analysis. Therefore, for a realistic analysis, it is suggested that elasto-visco-plastic behaviour be considered.
- Strain energy release rate is highly influenced by the adhesive properties, such as fluidity parameter and flow rule.
- Stress distributions, along the overlap length of the single lap joint, are predicted by the present elasto-visco-plastic analysis and the results are found to agree with those reported by Hiregoudar [11].
- Stress distributions, along the overlap length and across the adhesive thickness of the stepped lap joint, are predicted by the elasto-visco-plastic and the results agree with the those reported for thick adherend shear test (TAST) specimen by Su and Mackie [13].
- Strain energy release rate is sensitive to layup sequences in composite adherends. A proper choice of layup sequence in the composite adherend results in an efficient bonded joint.
- Use of adhesive of high fracture toughness, large overlap lengths and small thickness of adhesive individually results in a stronger bonded joint.

Acknowledgement

Financial support received from ISRO-RESPOND Scheme of the Department of Space, Govt. of India gratefully acknowledged.

REFERENCES

1. Groth, H. L. Calculation of stresses in bonded joints using the substructuring technique. *Int. J. Adhesion Adhesives* **6** (1), 31–35 (1986).
2. Biot, M. A. Theory of stress-strain relations in anisotropic viscoelasticity and relaxation phenomena. *J. Appl. Phys.* **25** (11), 1385–1391 (1954).
3. Zienkiewicz, O. C. and Cormeau, I. C. Visco-elasticity–plasticity and creep in elastic solids — A unified numerical solution approach. *Int. J. Numer. Methods Eng.* **8**, 821–845 (1974).
4. Zienkiewicz, O. C., Owen, D. R. J. and Cormeau, I. C. Analysis of viscoplastic effects in pressure vessels by the finite element method. *Nucl. Eng. Design* **28**, 278–288 (1974).
5. Kanchi, M. B., Zienkiewicz, O. C. and Owen, D. R. J. The visco-plastic approach to problems of plasticity and creep involving geometrical nonlinear effects. *Int. J. Numer. Methods Eng.* **12**, 169–181 (1978).
6. Schapery, R. A. Correspondence principles and a generalized J integral for large deformation and fracture analysis of viscoelastic media. *Int. J. Fract.* **25**, 195–223 (1984).
7. Owen, D. R. J. and Hinton, E. *Finite Elements in Plasticity*. Pineridge Press, Swansea, UK (1980).
8. Groth, H. L. Viscoelastic and viscoplastic stress analysis of adhesive joints. *Int. J. Adhesion Adhesives* **10** (3), 207–213 (1990).
9. Zienkiewicz, O. C. and Taylor, R. L. *The Finite Element Method*, 4th edn, Vol. 2. McGraw-Hill, New York (1991).

10. Pradhan, S. C., Iyengar, N. G. R. and Kishore, N. N. Parametric study of interfacial debonding in adhesively bonded composite joints. *Compos. Struct.* **29** (1), 119–125 (1994).
11. Hiregoundar, S. Viscoplastic and geometric nonlinear finite element analysis of adhesively bonded lap joint. M.Sc. Thesis Report, Dept. of Civil Engineering, Indian Institute of Science, Bangalore (1993).
12. Pradhan, S. C., Iyengar, N. G. R. and Kishore, N. N. Finite element analysis of crack growth in adhesively bonded joints. *Int. J. Adhesion Adhesives* **15** (1), 33–41 (1995).
13. Su, N. and Mackie, R. I. Two-dimensional creep analysis of structural adhesive joints. *Int. J. Adhesion Adhesives* **13** (1), 33–40 (1993).